Equivalent Circuit Approach for Practical Applications of Meander-Line Gratings

Molero Jimenez, Carlos; García-Vigueras, Maria; Rodríguez-Berral, Raúl; Mesa, Francisco; Llombart, Nuria

DOI
10.1109/LAWP.2017.2756438

Publication date
2017

Document Version
Accepted author manuscript

Published in
IEEE Antennas and Wireless Propagation Letters

Equivalent Circuit Approach for Practical Applications of Meander-Line Gratings

Carlos Molero, María García-Vigueras, Raúl Rodríguez-Berral, Francisco Mesa, *Fellow, IEEE*, and Nuria Llombart, *Senior Member, IEEE*

***Abstract*—This letter reports an analytical circuit model to characterize periodic arrangements of printed meander lines. The methodology employed for the derivation of the model is presented together with two typical examples of its possible application: a polarizer and an absorber. Comparisons with results provided by a commercial software evidence the good accuracy provided by the equivalent circuit.**

***Index Terms*—Absorbers, circuit models (CMs), meander lines, periodic structures, polarizers.**

I. Introduction

PERIODIC surfaces consisting of meander-line gratings (MLGs) have long been studied because they allow for the synthesis of specific anisotropic scattering. The basic underlying principle is that plane waves impinging on MLGs with electric field parallel to the meander-line axis experience an inductive behavior, whereas incident waves with perpendicular polarization encounter a capacitive sheet. Widely employed in the conception of polarizers, MLGs allow to convert the linear polarization of an impinging wave into circular. This solution was first proposed in 1970s [1], widely applied in successive years [2]–[4], with some approaches revisited nowadays for modern satellite communication systems [5]. MLGs can also find application in the design of dual-polarized absorbers. For instance, superconducting kinetic detectors in the terahertz/IR regime have been developed using linear absorbing strips [6], which were modeled analytically with the equivalent circuit presented in [7]. This geometry receives only one polarization, and instead the use of meandered absorbing mesh will allow the reception of two incoherent polarizations simultaneously increasing the overall system sensitivity and still be used as a resonating read out inductor.

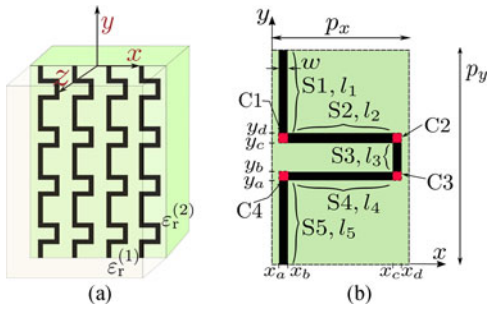

Fig. 1. (a) Sketch of the MLG and (b) front view of the unit cell. The meander is composed of five sections (named Si, with respective length l_i and $i = 1, \ldots, 5$) and four corner bends (marked in red and labeled as Ci with $i = 1, \ldots, 4$); $l_2 = l_4$, $l_1 = l_5$ so the full length of the meander can be, thus, approximated by $L = 2l_1 + 2l_2 + l_3 + 2w$.

Due to MLGs' potential and versatility, their characterization has also attracted much interest. Several models have already been reported in the literature [2], although their analytical formulation suffers from frequency and geometrical limitations. The present letter proposes a wideband equivalent circuit model (CM) that allows for the characterization of MLGs in layered media. The CM is based on some of the authors' previous works on physically insightful models [8], [9]. Analytical expressions can be provided for all the elements of the CM. A main requirement to build the CM is a good assumption of the meander surface-current distribution, which can be extracted either from standard method-of-moments entire-domain basis functions (such as those in [3]), or from commercial full-wave tools [8]. This CM is intended to be an efficient design tool for applications involving MLGs, here illustrated by means of two examples. This letter is organized as follows: Section II presents the general guidelines to build the CM, the way to obtain the surface current distribution on the meander, and the inclusion of ohmic/dielectric losses in the CM. Two applications of the CM are exposed in Section III, first a microwave polarizer and second a terahertz absorber. Numerical results provided by the CM are finally shown and compared to those obtained by CST [11] in order to validate the proposal.

II. MLG Circuit Model

The structure under study is sketched in Fig. 1(a), consisting of an MLG embedded by two semiinfinite dielectric media.

Manuscript received August 5, 2017; accepted September 5, 2017. Date of publication October 2, 2017; date of current version November 20, 2017. This work was supported in part by Rennes Métropole for the funds AIS 17C0481 and in part by Region Bretagne for the contract SAD 2016 9637 as well as the Spanish Ministerio de Economía y Competitividad with European Union FEDER funds (Project TEC2013-41913-P). *(Corresponding author: Carlos Molero.)*

C. Molero and M. García-Vigueras are with the Institut d'Electronique et de Télécommunications de Rennes (IETR), UMR CNRS 616, INSA Rennes, 35708 Rennes, France (e-mail: Carlos.Molero-Jimenez@insa-rennes.fr; maria.garcia-vigueras@insa-rennes.fr).

R. Rodríguez-Berral and F. Mesa are with the Department of Applied Physics 1, University of Seville, Seville 41012, Spain (e-mail: rrberral@us.es; mesa@us.es).

N. Llombart is with Microelectronics Department, Delft University of Technology, Delft 2628CD, the Netherlands (e-mail: n.llombartjuan@tudelft.nl).

Color versions of one or more of the figures in this letter are available online at http://ieeexplore.ieee.org.

The periodicity of the problem makes that the scattering of a plane wave impinging on this MLG can be analyzed by just considering its unit cell [sketched in Fig. 1(b)] and to interpret the scenario as a waveguide-discontinuity problem [8], [9]. The equivalent impedance for such a problem, Z_{MLG}, is next extracted following the guidelines reported in [9]. By imposing the scatterer's boundary conditions to the fields' Floquet expansions at both sides of the discontinuity, the following expression for Z_{MLG} can be derived [9, (49)]:

$$Z_{\mathrm{MLG}} = \frac{1}{\mathrm{j}\omega C_{\mathrm{ho}}} + \mathrm{j}\omega L_{\mathrm{ho}} + {\sum_{|n|,|m|\leq M}}' \frac{1}{|N_{nm}|^2[Y_{nm}^{(1)} + Y_{nm}^{(2)}]} \quad (1)$$

(the symbol $'$ in the summation implies that the incident harmonic is excluded). The resulting impedance represents the coupling of energy from the impinging wave to the rest of infinite higher-order (ho) Floquet harmonics of order n, m supported by the doubly-periodic MLG. Equation (1) is composed of three different contributions, all series connected from a circuital point of view (the equivalent circuit is displayed in [9, Fig. 8]). The first two contributions, the capacitance C_{ho} and the inductance L_{ho}, are related to the excitation of all evanescent TM and TE harmonics, respectively. These harmonics are characterized by an order $|n|$, $|m|$ greater than a certain integer number M. C_{ho} and L_{ho} can be expressed as ([9, (50) and (51)])

$$\frac{1}{C_{\mathrm{ho}}} = \frac{1}{\varepsilon_0(\varepsilon_{\mathrm{r}}^{(1)} + \varepsilon_{\mathrm{r}}^{(2)})} \sum_{|n|,|m|=M+1}^{\infty} \frac{|k_{n,m}|}{|N_{nm}^{\mathrm{TM}}|^2} \quad (2)$$

$$L_{\mathrm{ho}} = \frac{\mu_0}{2} \sum_{|n|,|m|=M+1}^{\infty} \frac{1}{|N_{nm}^{\mathrm{TE}}|^2 |k_{n,m}|} \quad (3)$$

with $k_{n,m}$ being the cutoff wavenumber of the harmonic of order n, m and $\varepsilon_{\mathrm{r}}^{(1)}$ and $\varepsilon_{\mathrm{r}}^{(2)}$ the relative permittivity of the media (1) and (2) [left and right sides of the discontinuity in Fig. 1(a)]. Each term included in the summations is weighted by a factor $N_{nm}^{\mathrm{TE/TM}}$, which is related to the projection of the transverse field profile of a TE/TM harmonic over the surface current density on the meander, named as $\mathbf{J}^{\mathrm{TE/TM}}(x, y)$. Detailed information on the nature and closed-form expression of this projection is available in [9] (see (32) in there). Both C_{ho} and L_{ho} are independent on the frequency and the angle of incidence, therefore they can be calculated once and stored. The third contribution in (1) corresponds to the excitation of the rest of harmonics of order $|n|$, $|m| \leq M$ that were not considered in the two previous regular reactance terms. Each term taking part in the summation corresponds to the the parallel connection of the frequency-dependent modal admittances $Y_{nm}^{(i)}$ of the harmonic under consideration (TE or TM) at each side of the discontinuity [medium (1) or (2)], weighted again by the corresponding factor $N_{nm}^{\mathrm{TE/TM}}$.

A. Analytical Expression for the Meander Surface Current

At operation wavelengths relatively larger or similar to the meander length L [see Fig. 1(b)], it can be assumed that the surface current density on MLGs does not vary significantly with frequency [8], [9]. Under this premise, a frequency-independent spatial profile can be defined for the surface current density. We propose the following analytical expressions for the spatial profile, which allow to consider TE/TM-polarized plane wave excitation of the MLG under conical incidence (i.e., from angles θ, ϕ):

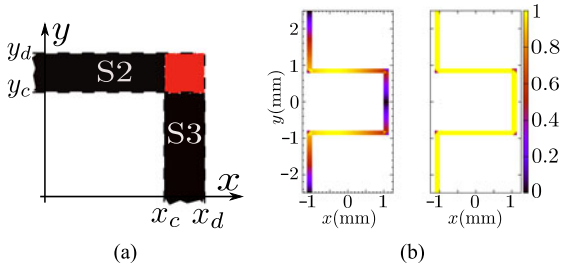

Fig. 2. (a) Detail of the corner bend formed by the strip sections S2 and S3. (b) Analytical surface-current profiles $\mathbf{j}_x$ (left) and $\mathbf{j}_y$ (right) computed for a given geometry.

$$\mathbf{j}^{\mathrm{TE}}(x, y) = [\sin(\phi)\, \mathbf{j}_x - \cos(\phi)\, \mathbf{j}_y]\, \mathrm{e}^{-\mathrm{j}k_{x0}x - \mathrm{j}k_{y0}y} \quad (4)$$

$$\mathbf{j}^{\mathrm{TM}}(x, y) = [\sin(\phi)\, \mathbf{j}_y + \cos(\phi)\, \mathbf{j}_x]\, \mathrm{e}^{-\mathrm{j}k_{x0}x - \mathrm{j}k_{y0}y}\,. \quad (5)$$

Here, the exponential functions depending on the transverse wavenumbers of the incident wave, $k_{x0} = k_0 \sin(\theta)\cos(\phi)$ and $k_{y0} = k_0 \sin(\theta)\sin(\phi)$, represent the phase shift imposed by the obliquely incident wave over the surface-current pattern. In these equations, $\mathbf{j}_{x/y}$ represent the current profiles excited in the meander by the x/y-directed components of the incident electric field. These profiles can be expressed by the following analytical expressions [the geometrical parameters of the meander are defined in Fig. 1(b)]:

$$\frac{\mathbf{j}_x}{\sqrt{2}} = \begin{cases} \sin\left(2\pi[y_c + l_2 + 2w + y - y_d]/L\right)\hat{\mathbf{y}}, & \mathrm{S1} \\ \sin\left(2\pi[y_c + w + x_c - x]/L\right)\hat{\mathbf{x}}, & \mathrm{S2} \\ \sin\left(2\pi y/L\right)\hat{\mathbf{y}}, & \mathrm{S3} \\ \sin\left(2\pi[y_b - w + x - x_c]/L\right)\hat{\mathbf{x}}, & \mathrm{S4} \\ \sin\left(2\pi[y_b - 2w - l_2 - y_a + y]/L\right)\hat{\mathbf{y}}, & \mathrm{S5} \end{cases} \quad (6)$$

$$\mathbf{j}_y = \begin{cases} \hat{\mathbf{y}}, & \mathrm{S1,\ S3,\ and\ S5} \\ -\hat{\mathbf{x}}, & \mathrm{S2} \\ \hat{\mathbf{x}}, & \mathrm{S4}\,. \end{cases} \quad (7)$$

These expressions are chosen starting from the basis functions for meander lines proposed in [3] and aim at preserving continuity between adjacent strips of the meander. Equation (6) implies a sine-shaped current profile when the impinging electric field is perpendicular to the meander (directed along x), and (7) a constant profile when the incident field is parallel to the meander (y-polarized). These profiles are assumed to be constant within the width w of the meander. Surface currents in (6) and (7) only cover the meander sections, not the corners [red square regions in Fig. 1(b)].

We define the current profiles in these corners so that they satisfy the boundary conditions imposed on the corner edges and preserving continuity between sections. The followed procedure is next illustrated for the case of the profile $\mathbf{j}_x$ in the corner formed between the meander sections S2 and S3, zoomed in Fig. 2(a). This profile is labeled as $\mathbf{j}_x^{23}$ and, considering (6), is taken as the following superposition of the current entering from

S2 and the surface current departing toward S3:

$$\mathbf{j}_x^{23} = \frac{\sqrt{2}}{w}\left[(x_d - x)\sin\frac{2\pi(y_c + w)}{L}\hat{\mathbf{x}} + (y_d - y)\sin\frac{2\pi y_c}{L}\hat{\mathbf{y}}\right]. \tag{8}$$

The x-directed component of (8) corresponds to the current coming from S2, flowing from x_c to x_d [see Fig. 2(a)]. The value of this component equals $|\mathbf{j}_x|$ in (6) for S2 when $x = x_c$, and it decays linearly with x, being null at the edge limit $x = x_d$. This zero value ensures that no perpendicular current exists at the corner edge. Applying the same rationale, the component in (8) directed along y is equal to $|\mathbf{j}_x|$ for S3 in (6) when $y = y_c$, and it is null at the edge $y = y_d$. This same procedure is applied for $|\mathbf{j}_y|$ and the rest of the corners bends. The resulting final vertical and horizontal current profiles are displayed in Fig. 2(b).

B. Incorporation of Ohmic and Dielectric Losses

Dielectric losses can be directly included in the proposed CM by considering the complex-valued permittivity of the substrate in the formulation. Here we extend the procedure in [9] to account for ohmic losses since they play a fundamental role in the characterization of absorption in MLGs. Reference [9, (33)], which described the null power consumption in a lossless metallic patch, should now be rewritten as

$$\int_\Omega \mathbf{J}^* \cdot \mathbf{E}\,\mathrm{d}\Omega = R_\mathrm{s}\int_\Omega \hat{\mathbf{z}} \times [\mathbf{H}^{(1)} - \mathbf{H}^{(2)}]\,\mathrm{d}\Omega \tag{9}$$

where R_s is the resistance in ohms-per-square, expressed in terms of the conductivity σ and thickness h of the metal, $R_\mathrm{s} = 1/(\sigma h)$ if weak skin effect is assumed. Additionally, $\mathbf{E}$ represents the electric field at either side of the discontinuity, and $\mathbf{H}^{(1)}$ and $\mathbf{H}^{(2)}$ are the magnetic field at each side of the discontinuity. After some manipulations, the following effective resistance, series connected to the elements in (1), can be recognized

$$R = R_\mathrm{s}\sum_{\forall n,m}\frac{1}{|N_{nm}|^2} \tag{10}$$

with the summation involving all the TE and TM harmonics.

III. Results

A. Stacked MLGs Used as Polarizers

Circular polarization can be achieved from MLGs by illuminating them with a $\phi = 45^\circ$ slant-polarized beam [1]. This way, the external excitation is regarded as the superposition of in-phase vertically and horizontally polarized (v/h-pol) plane waves of equal amplitude. An example of such structure consisting of a stack of three MLGs can be found in [4], whose unit cell is sketched at the top of Fig. 3. As the MLGs are spaced approximately $\lambda/4$ at the operation frequency, it can be considered that the reactive field in the vicinity of a single MLG is not affected by the presence of others. This assumption allows for the characterization of the structure by a CM based on a stack of Z_MLG as the ones presented in (1). Since the operation frequency is far below the onset of grating lobes, the excitation of all high-order harmonics in (1) is well captured by the elements C_ho and L_ho, with them being computed in (2) and (3) taking $M = 0$. The particular value taken by these circuit elements is

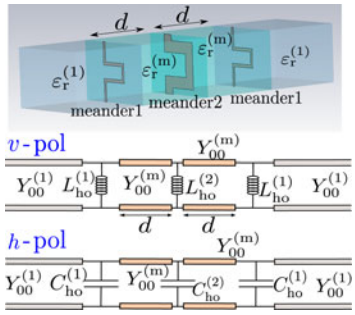

Fig. 3. Stacked-MLG polarizer and its equivalent CM when considering either vertical or horizontal illumination (y/x-directed impinging electric field).

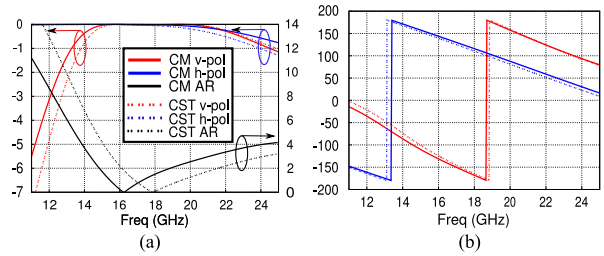

Fig. 4. (a) S_{21} magnitude (left axis) and AR (right axis), both in decibels. (b) S_{21} phase (degrees). Structure dimensions are taken from [4, Table I].

strongly influenced by the polarization of the impinging wave, being possible to identify different simplified CMs for the v-pol and for the h-pol cases. When the impinging electric field is v-pol (directed along y), the current profile excited in the MLG is that in (7), giving rise to a null capacitive impedance when computing (2) and, thus, an inductive equivalent impedance Z_MLG. When the impinging electric field is h-pol (directed along x), the current profile in (6) is considered, resulting in nonzero inductive and capacitive terms (with the capacitive contribution being the dominant one). Here, the inductive contribution depends strongly on the length of the meander horizontal strips [parameters l_2 and l_4 in Fig. 1(b)]. When those strips are short, as in our case of study [4] and most of MLG polarizers, L_ho becomes negligible. The resulting CM for each polarization is displayed in Fig. 3, showing that the CM is mainly inductive/capacitive for v/h-excitation of the MLGs. The transmission lines characterize the propagation of the incident fundamental harmonic between MLGs.

The magnitude and phase of the polarizer transmission coefficient (S_{21}) for v/h-incidence, together with the axial ratio (AR), are plotted in Fig. 4 comparing the CM and CST results. From Fig. 4(a), it can be inferred the existence of total transmission bands between 16 and 18 GHz for both polarizations, as well as from Fig. 4(b) an almost 90° phase difference between them along the same band. The purity of circular polarization is better accounted for by the AR, displayed in Fig. 4(a); high purity is usually associated with values below 3 dB. This value is reached by the polarizer under study, though here the results provided by the CM and CST differ slightly. This deviation stems mainly from the the high sensitivity intrinsic to the definition of the AR. Note that any minor discrepancies in the S_{21} magnitude or phase will strongly impact the AR agreement. All in all, it is important to note that the behavior of the polarizer

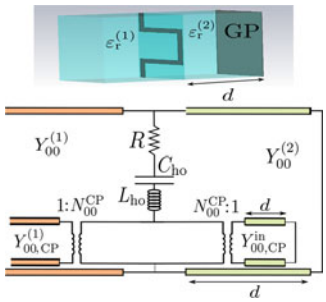

Fig. 5. Structure of an MLG used as an absorber when backed by a GP, and its equivalent CM (ohmic losses and excitation of the cross-pol is here explicitly considered). Dimensions in μm: $p_y = 24.6$, $p_x = 16.5$, $w = 1.58$, $\Delta x = 0.544$, $l_y = 10.40$, and $d = 20.8$. The media permittivities are $\varepsilon_r^{(1)} = \varepsilon_r^{(2)} = 11.9$ and $R_s = 7.7\,\Omega/\text{sq}$.

is reasonably well captured by the CM, additionally providing a good physical insight into its underlying operation mechanism.

B. Metal-Backed MLGs Used as Absorbers

On the basis of the Salisbury's screen technique [10], absorbers can be conceived by placing an MLG at a distance around $\lambda/4$ from a ground plane (GP). The advantage of using meander geometries lies in the possibility of controlling the absorption associated with v- and h-pol independently. In order to achieve an efficient absorption level, the resistive properties of the metallic meander have to be conveniently tuned. A picture of the structure and its corresponding CM is shown in Fig. 5. In order to include the presence of the GP in the CM, each of the transmission lines associated with the propagation along the grounded dielectric slab [medium (2)] has to be short-circuited. This way, the modal admittances $Y_{nm}^{(2)}$ in (1) are replaced with

$$Y_{nm}^{\text{in}} = -\text{j}Y_{nm}^{(2)} \cot\left(\beta_{nm}^{(2)} d\right) \tag{11}$$

where $\beta_{n,m}^{(2)}$ is the propagation constant of the nm-harmonic inside the grounded dielectric, and d is the thickness of the grounded substrate. Absorption operation is more efficient when working well below the onset of grating lobes, and in this situation the CM can be simplified by accounting for the contribution of all high-order harmonics by regular inductive and capacitive terms. In contrast to the previous example, the possibility to excite the cross-pol term is now considered, which appears under conical incidence (out from the principal planes). In the CM shown in Fig. 5, the resistance R associated with the ohmic losses is also included following the procedure in Section II-B. The proposed CM not only helps us understand the absorber operation, but also to speed up its design to match any specific practical requirement. The example described in Fig. 5 has been designed so that the absorption band takes place in the terahertz regime, addressing the specifications demanded for LEKID devices [6]; some results are presented in Fig. 6. The absorption band achieved for each polarization in Fig. 6(a) and (b) is quite wide, assuming the value -3 dB as the band limit. The results for conical incidence plotted in Fig. 6(c) and (d) highlight that the absorption performance is not only kept but enhanced. The results provided by the proposed model are, generally, in good agreement with those obtained with CST, confirming again its usefulness for thoughtful design.

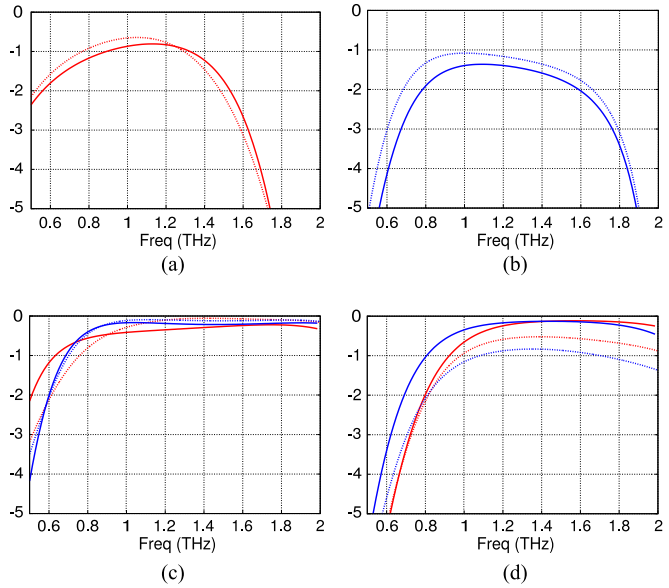

Fig. 6. Absorption coefficient (dB) when incidence is: (a) normal v-pol, (b) normal h-pol, (c) conical TE (red lines correspond to $\theta = 45°$, $\phi = 30°$, and blue lines to $\theta = 45°$, $\phi = 45°$), and (d) conical TM where blue and red lines represent the same as in (c). Solid/dotted lines correspond, respectively, to CM/CST results.

IV. Conclusion

An analytical CM for MLGs has been presented and proposed as a design tool. The circuit is applied for the design of absorbers and polarizers. The results provided by the CM show a very good performance after being compared with results provided by CST.

References

[1] L. Young, L. A. Robinson, and C. A. Hacking, "Meander-line polarizer," *IEEE Trans. Antennas Propag.*, vol. AP-21, no. 3, pp. 376–378, May1973.

[2] C. Terret, J. R. Levrel, and K. Mahdjoubi, "Susceptance computation of meander-line polarizer layer," *IEEE Trans. Antennas Propag.*, vol. AP-32, no. 9, pp. 1007–1011, Sep. 1984.

[3] A. K. Bhattacharyya and T. J. Chwalek, "Analysis of multilayered meander line polarizer," *Int. J. Microw. Millim.-Wave Comput.-Aided Eng.*, vol. 7, no. 6, pp. 442–454, 1997.

[4] M. A. Joyal, M. Riel, Y. Demers, and J. J. Laurin, "A meander-line circular polarizer optimized for oblique incidence," *IEEE Trans. Antennas Propag.*, vol. 63, no. 12, pp. 5391–5398, Dec. 2015.

[5] A. Ericsson and D. Sjoberg, "Design and analysis of a multilayer meander line circular polarization selective structure," *IEEE Trans. Antennas Propag.*, vol. 65, no. 8, pp. 4089–4101, Aug. 2017.

[6] S. Doyle, "Lumped element kinetic inductance detector," Ph.D. dissertation, Department of Physics and Astronomy, Cardiff Univ., Cardif, U.K., Apr. 2008.

[7] B. Blázquez, N. Llombart, D. Cavallo, A. Freni, and A. Neto, "A rigorous equivalent network for linearly polarized THz absorbers," *IEEE Trans. Antennas Propag.*, vol. 62, no. 10, pp. 5077–5088, Oct. 2014.

[8] F. Mesa, M. García-Vigueras, F. Medina, R. Rodríguez-Berral, and J. R. Mosig, "Circuit model analysis of frequency selective surfaces with scatterers of arbitrary geometry," *IEEE Antennas Wireless Propag. Lett.*, vol. 14, pp. 135–138, 2015.

[9] R. Rodríguez-Berral, F. Mesa, and F. Medina, "Analytical multimodal network approach for 2-D arrays of planar patches/apertures embedded in a layered medium," *IEEE Trans. Antennas Propag.*, vol. 63, no. 5, pp. 1969–1984, May 2015.

[10] W. W. Salisbury, "Absorbent body for electromagnetic waves," U.S. Patent 2 599 944, Jun. 1952.

[11] CST Microwave Studio, 2017. [Online]. Available: https://www.cst.com/products/cstmws